Synthetic Agonist of Growth Hormone-Releasing Hormone as Novel Treatment for Heart Failure with Preserved Ejection Fraction

Raul A. Dulce[1], Rosemeire M. Kanashiro-Takeuchi[1,2], Lauro M. Takeuchi[1], Alessandro G. Salerno[1], Shathiyah Kulandavelu[1,6], Wayne Balkan[1,3], Marilia S.S.R. Zuttion[1], Renzhi Cai[4], Andrew V. Schally[3,4,5] and Joshua M. Hare[1,3]*

Affiliations:

[1]Interdisciplinary Stem Cell Institute, University of Miami Miller School of Medicine, Miami, Florida 33136, USA.

[2]Department of Molecular and Cellular Pharmacology, University of Miami Miller School of Medicine, Miami, Florida 33136, USA.

[3]Department of Medicine, University of Miami Miller School of Medicine, Miami, Florida 33136, USA.

[4]Endocrine, Polypeptide and Cancer Institute, Veteran Affairs Medical Center, Florida 33136, USA.

[5]Division of Hematology/Oncology, University of Miami Miller School of Medicine, Miami, Florida 33136, USA.

[6]Department of Pediatrics, University of Miami Miller School of Medicine, Miami, Florida 33136, USA.

***Corresponding Author:** Joshua M. Hare, M.D. Director, Interdisciplinary Stem Cell Institute. Biomedical Research Building, 1501 N.W. 10th Avenue, Room 924, Miami, FL 33136, USA. Phone: +1-305-243-1999; Fax: +1-305-243-3906. Email: jhare@med.miami.edu.

Abstract

Heart failure with preserved ejection fraction (HFpEF) is characterized by a myocardium with impaired relaxation, fibrosis and ventricular stiffness. Despite the rapidly increasing prevalence of HFpEF, no effective therapies have emerged. Here we show that a potent synthetic agonist of growth hormone-releasing hormone (GHRH-A) both prevents and reverses the HFpEF phenotype generated in mice through continuous infusion of angiotensin-II (Ang-II). Animals treated with Ang-II had diastolic dysfunction, and isolated cardiomyocytes (ex vivo) exhibited incomplete relaxation, depressed contractile responses and altered myofibrillar protein phosphorylation. Calcium handling mechanisms were disturbed in cardiomyocytes from mice with HFpEF. The GHRH-A MR-356 prevented the development of the pathological phenotype and reversed the phenotype in vivo and ex vivo in mice with established HFpEF. Taken together these findings indicate that the GHRH receptor signaling pathway represents a new molecular target to counteract HFpEF-associated cardiomyocytye dysfunction by targeting myofilament phosphorylation. Accordingly, activation of the GHRH receptor with potent synthetic GHRH agonists may provide a novel therapeutic approach to management of HFpEF syndrome.

43 Heart failure (HF) remains a leading cause of death worldwide and is associated with two
44 general clinical variants - heart failure with reduced ejection fraction (HFrEF), characterized by
45 systolic dysfunction, and heart failure with preserved ejection fraction (HFpEF), predominantly
46 due to diastolic dysfunction[1-3]. HFpEF accounts for ~50% of HF cases, a proportion that is
47 predicted to increase at about 1% per year relative to HFrEF[4, 5]. Whereas there are numerous
48 approved and guideline supported drugs for HFrEF, there are no approved therapies targeting
49 HFpEF, and numerous clinical trials with several classes of drugs have failed to produce clinical
50 benefits[6-10]. The HFpEF syndrome is characterized by endothelial dysfunction, hypertension,
51 impaired relaxation and contractile reserve, ventricular stiffening and fibrosis[2, 11, 12]. The
52 underlying molecular mechanisms of HFpEF are poorly understood due to its diverse etiology,
53 which in most cases involves multi-organ pathological conditions[13-15]. Importantly, current
54 therapeutic strategies fail to stop the progression of HFpEF[6, 8, 16-18], creating a healthcare crisis
55 due to the unmet therapeutic need for HFpEF patients[19, 20].

56 The development of new potent synthetic growth hormone-releasing hormone agonists
57 (GHRH-As) and their application in different models of myocardial injury (either ischemic[21-25]
58 or non-ischemic[26]) demonstrates the effectiveness of myocardial GHRH receptors (GHRHRs)
59 activation to reduce fibrosis or hypertrophy, respectively, and improve cardiac performance[22-26].
60 The signaling of GHRHR extends beyond the hypothalamic-pituitary axis[27] as the GHRHRs are
61 present on cardiomyocytes[22, 23]. Based upon the effects of GHRH-As on myocardial fibrosis,
62 hypertrophy and performance, we hypothesized they would improve cardiomyocyte function in
63 HFpEF.

64 Among the limited number of animal models that reproduce the features of HFpEF
65 observed in humans[14, 28-31], chronic infusion of a low dose of angiotensin II (Ang-II) in mice,
66 reproduces the HFpEF cardiac phenotype in the absence of elevated systemic arterial blood
67 pressure[32]. We used this model to study the effects of a GHRH-A, MR-356, on the performance
68 of cardiomyocytes *ex vivo* and *in vivo*. Synthetic MR-356 is about 150 times more potent[21] than
69 human GHRH(1-29)NH_2 and binds to the GHRHR with 7.5 fold greater affinity. Here we tested
70 the hypotheses that activation of GHRHR signaling within the myocardium both prevents and
71 reverses myocardial HFpEF features in vivo through mechanisms involving both myocardial
72 fibrosis and impaired cardiomyocyte relaxation.

73

74 **Results.**

75 *GHRH-A prevents the appearance of the HFpEF syndrome induced by in vivo Ang-II*
76 *infusion.*

77 Four-weeks of continuous infusion of Ang-II induced a cardiovascular phenotype that
78 mimicked the phenotypic features of HFpEF[32]. Specifically, Ang-II-treated mice exhibited
79 myocardial hypertrophy with increased heart weight normalized by body weight or tibia length
80 (Figure 1A and Online Supplemental Table 1), increased relative wall thickness in diastole
81 (RWTd) and increased cardiomyocyte width (Figure 1B-C) without changes in length (Online
82 Supplemental Figure 1). Myocardial fibrosis was increased in the HFpEF hearts as evidenced by
83 collagen III content, the transforming growth factor-β (TGF-β, a fibrosis mediator) and the
84 myofibroblast biomarker α-smooth muscle actin (α-SMA) (Figure 1D-F). We also observed a
85 trend to increase both the prolyl-4-hydroxylase-α-1 (P4HA1, a key enzyme for the hydroxylation
86 of proline residues on collagen), and the hydroxyproline residues (a modified amino acid residue
87 characteristic of the collagen primary structure) (Online Supplemental Figure 2A-B). Whereas
88 collagen I and vimentin (a biomarker for undifferentiated fibroblasts) did not change (Online
89 Supplemental Figure 2C-D). Co-administration of the GHRH analog, MR-356 prevented the
90 increases in RWTd and cardiomyocyte width seen in the Ang-II treated group (Figure 1B-C).
91 Moreover, MR-356 treatment protected against fibrosis, since collagen III content, TGF-β and α-
92 SMA levels were reduced (Figure 1D-F).

93 Echocardiographic evaluation demonstrated that Ang-II infusion did not reduce ejection
94 fraction (EF) (Online Supplemental Tables 2), either alone or under co-treatment with MR-356.
95 Likewise, chamber dimensions were unaffected in systole between groups (Supplemental Table
96 2). Using invasive hemodynamic assessment (Table 1), we found increased arterial blood
97 pressure, a characteristic of HFpEF, and clear evidence of diastolic dysfunction with increased
98 end-diastolic pressure-volume relationship (EDPVR) (Figure 2A-D), relaxation time constant
99 (tau) and left ventricular end-diastolic pressure (LVEDP) in Ang-II-treated mice compared to
100 control (Figure 2E-F). Isovolumic relaxation time (IVRT) increased along the time course of the
101 treatment (Figure 2H) (within group comparison - 4-week versus baseline), and this increase was
102 greater in the Ang-II-treated group (as compared versus controls at 4-week time point) consistent
103 with the initial description of this model[32]. Global longitudinal strain (GLS) increased (a

104 reduction in absolute values) with Ang-II treatment, similar to that observed in diastolic
105 dysfunction[33] (Figure 2I and Supplemental Table 2). Co-infusion of MR-356 completely
106 prevented the development of diastolic dysfunction (Figure 2C-I) and induced a robust
107 acceleration in dP/dt_{min} (Figure 2G). Taken together, these results demonstrate that stimulation of
108 GHRH pathway with the potent agonist MR-356 effectively counteracted the development of
109 HFpEF induced by Ang-II.

110 *GHRH-A prevents sarcomere and contractile dysfunction in HFpEF cardiomyocytes*

111 In order to test whether GHRH agonists directly affect cardiomyocyte function, we
112 studied cardiomyocytes isolated from Ang-II-treated mice, which were electric field-stimulated
113 at 1, 2 and 4 Hz. They exhibited shorter resting sarcomere length compared to those from control
114 animals (Figure 3A and B), indicating an inability to relax, consistent with HFpEF[11, 32].
115 Quiescent HFpEF cardiomyocytes exposed to 1.8 mmol/L extracellular $CaCl_2$ were consistently
116 shorter compared to control cardiomyocytes, while there was no difference between groups in
117 Ca^{2+}-free buffer in the presence of 2,3-butanedione monoxime (BDM) (Online Supplemental
118 Figure 3A). HFpEF cardiomyocytes also exhibited depressed contractile response to pacing
119 (Figure 3A and C). However, concomitant treatment with MR-356 during Ang-II infusion, not
120 only prevented the impairment in sarcomere tension at resting intervals between twitches at all
121 frequencies (Figure 3A and B), but also preserved quiescent cardiomyocyte length in the
122 presence of extracellular Ca^{2+} (Online Supplemental Figure 3A, right panel). Treatment with
123 MR-356 also preserved sarcomere shortening and response to pacing at levels equivalent to those
124 in control cardiomyocytes (Figure 3A and C). Paradoxically, shorter sarcomere length in HFpEF
125 cardiomyocytes were associated with lower $[Ca^{2+}]$ at resting intervals (Figure 3D and E, p=0.028
126 compared with controls), which was prevented by treatment with MR-356. These findings
127 suggest a possible alteration in sensitivity of myofilaments for Ca^{2+}. There were no significant
128 differences in Ca^{2+} transient amplitude ($\Delta[Ca^{2+}]$) between groups (Figure 3D and F), but there
129 was a positive response to pacing in peak $[Ca^{2+}]$ in control cardiomyocytes while HFpEF
130 cardiomyocytes exhibited a depressed response (Online Supplemental Figure 3B). MR-356
131 reestablished the increasing $[Ca^{2+}]$-frequency relationship (Online Supplemental Figure 3B-C),
132 which is clearly shown by the normalized $\Delta[Ca^{2+}]$ in response to pacing, with respect to their
133 amplitude at 1 Hz (Figure 3G). The HFpEF cardiomyocytes exhibited a flat response compared
134 with the other groups (p<0.01), which correlates with their contractile response (Figure 3C).

135 In order to further characterizing this abnormal response of intracellular Ca^{2+} to pacing,
136 we assessed sarcoplasmic reticulum (SR) Ca^{2+} leak by using tetracaine (see Supplemental
137 methods and Figure 4A) and studied the SR Ca^{2+} leak-load relationship in cardiomyocytes.
138 Increased SR Ca^{2+} leak is a hallmark of heart failure. We found that Ang-II-treated myocytes
139 exhibited a steeper rise compared with controls ([Ca^{2+}] constants $\mathbf{k}_{AngII}$=0.0117±0.0011 μmol^{-1}.L
140 vs. $\mathbf{k}_{control}$=0.0047±0.0029 μmol^{-1}.L, $p<0.05$) and, although it remained elevated at low SR Ca^{2+}
141 loads, the load-leak curve was flattened by treatment with MR-356 ($\mathbf{k}_{AngII+MR-356}$=0.0016±0.0009
142 μmol^{-1}.L, $p<0.0001$ vs. Ang-II-HFpEF; Figure 4B). Thus, at matched SR Ca^{2+} load (SR Ca^{2+}
143 load =99.1±11.5 μmol/L), the Ca^{2+} leak was elevated in Ang-II-induced HFpEF cardiomyocytes
144 and partially prevented by treatment with MR-356 (Figure 4C).

145 *Effect of GHRH-A on the impaired Ca^{2+} decline in HFpEF cardiomyocytes*

146 This murine model of HFpEF is associated with a subtle but consistent reduction in Ca^{2+}
147 decay rate. We compared the time to different phases of the Ca^{2+} decay (time to 10%, tt10; time
148 to 50%, tt50; tau and time to 90%, tt90). At 1 Hz, we found slower [Ca^{2+}] decay in HFpEF
149 cardiomyocytes compared with controls (Figure 5A and B). Treatment with MR-356 blocked the
150 delayed Ca^{2+} decline at tt90% in the Ang-II+MR-356 (Figure 5A and B). The main mechanism
151 involved in Ca^{2+} decay in mice is the re-uptake into the SR. Despite the slower Ca^{2+} decay in
152 Ang-II-treated cardiomyocytes, the Ca^{2+} content in the SR, estimated by a rapid caffeine pulse,
153 was not reduced compared to control. Ang-II+MR-356 co-treatment did increase the SR [Ca^{2+}]
154 in comparison to control cardiomyocytes (Figure 5C). To elucidate the molecular mechanisms
155 involved in such effects, we investigated the proteins participating in Ca^{2+} handling. Re-uptake
156 of cytosolic Ca^{2+} into the SR occurs through the SR Ca^{2+} ATPase, SERCA2. There was reduced
157 expression of SERCA2a protein in cardiomyocytes from Ang-II-treated mice (Figure 5D).
158 Phospholamban (PLB), a small Ca^{2+}-cycling regulatory protein that exerts an inhibitory effect on
159 SERCA2 by protein-protein interaction, can be phosphorylated at serine 16 (p-Ser16) or
160 threonine 17 (p-Thr17), and so releasing the repression on SERCA2a activity. We observed
161 increased p-Ser16 and p-Thr17 PLB following Ang-II treatment, which was further increased by
162 co-treatment with MR-356 (Figure 5E and F). We also assessed the protein expression of a
163 subunit of the L-type Ca^{2+} channel (L-TCC 1αC), an important voltage-induced entrance of Ca^{2+}
164 to the cardiomyocyte, which plays a main role in the excitation-contraction coupling. L-TCC

165 1αC was increased by Ang-II, suggesting a possible Ca^{2+} overload in the HFpEF model. MR-356
166 treatment partially prevented this molecular change (Online Supplemental Figure 4A). The
167 electrogenic Na^{+}/Ca^{2+} exchanger (NCX) plays a discrete role in the Ca^{2+} decay rate in murine
168 cardiomyocytes, but is primarily responsible for Ca^{2+} removal. NCX gains relevance under some
169 pathologic heart conditions, where its expression may appear to be up-regulated. We tested
170 protein expression of the cardiac isoform, NCX1, which was unchanged by Ang-II treatment but
171 was reduced by MR-356 co-treatment compared with control cardiomyocytes (Online
172 Supplemental Figure 4B).

173 *Impaired cardiomyocyte relaxation in HFpEF is improved by GHRH-A*

174 Myocardial stiffness and deficient relaxation are hallmarks of the HFpEF syndrome,
175 which may be due to factors external to the cardiomyocyte, such as fibrosis, or intrinsically
176 associated with sarcomeric proteins, such as defects in titin structure/function or changes in
177 sensitivity of myofilaments to Ca^{2+}. At the cardiomyocyte level, this Ang-II-induced HFpEF
178 model exhibited reduced ability to relax mainly during the latter part of the relaxation phase (tau
179 and tt90%, Figure 6A and B) in a greater extent than our observations on Ca^{2+} decay. Treatment
180 with MR-356 not only prevented the prolongation of these parameters in the Ang-II-treated
181 model, but also significantly improved all phases of sarcomere relaxation at all frequencies
182 (Figure 6A and B). The exaggerated effect of MR-356 on sarcomere relaxation in comparison
183 with that on Ca^{2+} cycling might imply direct targeting of myofilament proteins. Faster relaxation
184 is associated with desensitization of myofilaments to Ca^{2+}. Accordingly, we analyzed SL-[Ca^{2+}]
185 hysteresis loops of cardiomyocyte contractions induced by electric-field stimulation, in order to
186 detect differences in responsiveness to Ca^{2+}. In general terms, the morphology of the loops was
187 greatly affected in the HFpEF model (Figure 6C). In the relaxation phases (Figure 6C and D
188 left), there was chronic Ang-II-induced sensitization of myofilaments ($p<0.0001$, Figure 6D
189 right) consistent with the delayed Ca^{2+} decline in this HFpEF model. As expected, co-treatment
190 with MR-356 induced a robust desensitizing effect that correlated with the exacerbated lusitropic
191 effect of MR-356 on isolated cardiomyocytes (Figure 6D). Cardiac troponin I (cTnI) plays an
192 important role in regulating responsiveness of myofilaments to Ca^{2+}, and its phosphorylation is a
193 determining factor in the affinity of troponin C (TnC) for Ca^{2+}. We explored phosphorylation on
194 sensitive sites of cTnI with regulatory activity, serine 23/24. TnI phosphorylation was slightly
195 impaired in Ang-II-treated cardiomyocytes (p=0.071) while co-treatment with MR-356 promoted

196 increased phosphorylation (Figure 6E) showing a consistent correlation with the data of
197 responsiveness to Ca^{2+} in panel 6D. Myosin binding protein C (MyBPC) contributes
198 substantially in cross-bridge cycling and its phosphorylation is also a main regulator of
199 myofilament sensitivity[34, 35]. HFpEF cardiomyocytes exhibited depressed phosphorylation at
200 serine 282, but no alteration in phosphorylation was detected in cardiomyocytes of animals
201 treated with Ang-II+MR-356 (Figure 6F).

202 *GHRH-A prevents impairment of the activation (contraction) phase of SL–[Ca^{2+}] loops*
203 *in HFpEF cardiomyocytes*

204 An evident negative inotropism determined by lower dSL/dt_{max}, was seen in HFpEF
205 cardiomyocytes indicating a disturbed excitation-contraction coupling and MR-356 prevented
206 this effect (Supplemental Figure 5A). an alternative approach to further assess the interaction
207 Ca^{2+}-sarcomere shortening was through the analysis of the "force-activation" phase of the SL-
208 [Ca^{2+}] loops in order to demonstrate the effects of MR-356 at the level of cross-bridge cycling.
209 In accordance with the slower contraction rate induced by chronic Ang-II treatment, the slopes of
210 the activation phase were consistently reduced in HFpEF cardiomyocytes (Supplemental Figure
211 5B and C). This reduction indicates a deteriorated cross-bridge cooperativity (and contractile
212 performance) which was prevented by co-treatment with MR-356.

213 *GHRH-A improves relaxation and reverts the HFpEF phenotype induced by eight-week*
214 *Ang-II infusion in CD1 mice.*

215 Given the ability of GHRH-As to prevent the onset of HFpEF, we next performed
216 experiments to test whether GHRH-As reverses established HFpEF. Accordingly, we infused
217 mice with a low dose of Ang-II for 8 weeks and initiated either treatment with MR-356 or the
218 vehicle at week 4, once the HFpEF phenotype was already apparent. Ang-II infusions were
219 continued in both groups during the second 4-week period. In vivo hemodynamic assessments
220 revealed that MR-356 restored the EDPVR (Figure 7 A-C), as well as the relaxation time
221 constant (τ) (Figure 7D) and the LVEDP (Figure 7E) back towards normal in HFpEF animals.
222 On the other hand, the increase in IVRT during the first 4-week treatment with Ang-II in both
223 groups, showed a trend to continue increasing in the HFpEF group. This tendency appears to be
224 stopped or even reverted in the group treated with MR-356 (Figure 7F), although this effect was
225 not significant within the period of the study. The beneficial effects on diastolic function were

226 also present on isolated cardiomyocytes, since MR-356 restored the resting sarcomere length (in
227 diastole, Figure 7G-H). Moreover, sarcomere relaxation rate was accelerated by MR-356
228 treatment in comparison with the 8-week Ang-II group (Figure 7I), as represented by the traces
229 on Figure 7G. Treatment with MR-356 also reverted the delay in decay of Ca^{2+} as shown by the
230 tt50% in response to pacing, in consonance with the increased transcription (mRNA) of the gene
231 for SERCA2a (Supplemental Figure 6). Moreover, time to peak SL contraction (ttp) and tt50%
232 SL relaxation in response to pacing (Supplemental Figure 7A and B) were greatly improved by
233 MR-356 on HFpEF cardiomyocytes, which was associated with increased gene expression of
234 troponin I (TNNi1 and 3) and myosin heavy chain α (MHY6) (Supplemental Figure 7C-E).
235 Myocardial remodeling was also reverted by MR-356 in this model, at least in terms of the
236 reversal of the left ventricular hypertrophy (Supplemental Figure 8A) and the re-expression of
237 the fetal gene myosin heavy chain β (MHY7), since the ratio MHY6/MHY7 was substantially
238 increased (Supplemental Figure 8).

239

240 **Discussion**

241 Heart failure with preserved ejection fraction is a syndrome with rising incidence and
242 prevalence that is unresponsive to conventional treatments for heart failure with reduced ejection
243 fraction. Given the rising clinical burden, it is imperative that effective treatments are found.
244 Here we show that a novel class of peptide compounds, GHRH-As, previously shown to
245 ameliorate pathological myocardial remodeling, also possess a powerful effect to restore
246 diastolic dysfunction, a hallmark of HFpEF, to normal in an animal model of HFpEF, acting
247 broadly through mechanisms involving fibrosis as well as myocyte calcium cycling and
248 myofilament calcium responses.

249 Chronic administration of Ang-II reproduces structural and functional myocardial
250 changes associated with HFpEF in mice. In contrast to previous results published by Regan el
251 al.[32], we found signs of hypertension, as the blood pressure in the aorta was increased in these
252 Ang-II treated mice (Table 1). This present in the majority of patients with HFpEF and might
253 represent a risk factor[36]. These animals showed preserved EF and other contractility indices but
254 depressed overall function, as observed with GLS[33], and associated with elevated LVEDP,
255 myocardial fibrosis and impaired diastolic function as measured by IVRT, EDPVR and the
256 relaxation constant tau. Within this pathological context, HFpEF animals showed myocardial
257 hypertrophy that was virtually redirected into a physiological hypertrophy by treatment with
258 MR-356, since although the increase in heart mass was not prevented in mice co-treated with
259 Ang II+MR-356, cardiomyocyte width and diastolic RWT were maintained as in control mice as
260 well as the fibrosis markers and the overall myocardial performance. In consonance with this,
261 MR-356 reverted the left ventricular hypertrophy in the 8-week HFpEF model (Supplemental
262 figure 8A). Accordingly, our results show that the above-mentioned signs consistent with HFpEF
263 syndrome, were both prevented or reversed by the treatment with the GHRH-A.

264 Isolated cardiomyocytes from HFpEF mice exhibited lusitropic impairment as well as
265 alterations in Ca^{2+} handling consistent with deficient myocardial relaxation and diastolic
266 dysfunction. In this sense, our compelling experimental data suggest that the deficient
267 myofilament relaxation in HFpEF cardiomyocytes might be associated with higher affinity of
268 myofilaments for Ca^{2+}, favoring binding of cytosolic Ca^{2+} to TnC and thus promoting a delayed
269 release of the interaction between thin and thick filaments. This idea is supported by the finding

270 of myofilament sensitization in HFpEF cardiomyocytes (leftward shift in the relaxation phase of
271 SL-Ca^{2+} loops) associated with reduced phosphorylation of cTnI at serine 23/24 and cMyBPC at
272 serine 282. In this sense, Ca^{2+} bound to myofilaments represents a very high percentage of the
273 Ca^{2+} released from the SR in a typical heart beat (about 50%)[37]. Therefore, the increased affinity
274 of myofilaments for Ca^{2+} has a substantial impact on cytosolic [Ca^{2+}], being able to buffer large
275 amounts of Ca^{2+}, including the Ca^{2+} leaked from the SR in HFpEF cardiomyocytes, and therefore
276 reducing the detectable levels. Moreover, the higher affinity for Ca^{2+} would make slower its
277 detachment from the troponin complex, which would impact the cytosolic [Ca^{2+}] decay rate[38, 39].
278 The increased PLB phosphorylation in the HEpEF cardiomyocytes appears not being sufficient
279 to compensate against both, the mentioned effect of the higher affinity for Ca^{2+} of myofilaments
280 and the diminished SERCA2 expression. The enhanced phosphorylation induced by MR-356 on
281 PLB, together with the desensitization of myofilaments, counteracted more efficiently and
282 prevented Ca^{2+} decay rate to slow (as shown in Figure 5 for the 4-week HFpEF model and
283 Supplemental Figure 6 in the 8-week HFpEF model). Importantly, NCX1 working in a reverse
284 mode ($NCX1_{rev}$) can contribute to the slowing of the Ca^{2+} decay rate in our murine model of
285 HFpEF, since low concentrations of Ang-II indirectly induce such a mechanism[40] without
286 affecting its protein expression. A study using a rat model of chronic kidney disease
287 (nephrectomy), which exhibits characteristics of HFpEF[29], demonstrated a main role for this
288 $NCX1_{rev}$ in the setting of HFpEF. An inhibitor of the NCX1 (SEA400), both in vivo and in vitro,
289 abolished the typical alteration in myocardium relaxation and remodeling. In this regard, it may
290 be appropriate to note that SEA400 inhibits both NCX working modes, reverse and forward.
291 Consistently, in our study, co-treatment with MR-356 down-regulated NCX1 expression, which
292 would suggest a reduced $NCX1_{rev}$ activity in HFpEF+MR-356 animals. However, this effect of
293 MR-356 on NCX1 expression would also affect the forward mode of the exchanger, with the
294 consequent removal of less Ca^{2+} from the cardiomyocyte, which in our model, is evidenced by
295 the increased levels of intracellular Ca^{2+} (SR[Ca^{2+}]) in cells from mice treated with this GHRH-
296 A.

297 We observed that myofilament responsiveness to Ca^{2+} was greatly decreased in
298 cardiomyocytes from Ang-II+MR-356-treated mice. This lower affinity of myofilaments for
299 Ca^{2+} may not only explain the molecular basis for faster relaxation, but also be the reason why
300 treatment with MR-356 preserved diastolic [Ca^{2+}] in Ang-II-treated myocytes; i.e., by preventing

301 the increase in Ca^{2+} buffering capacity of myofilaments. It has been demonstrated that this
302 molecular mechanism facilitates Ca^{2+} dissociation from cardiac myofilaments in response to
303 increasing pacing by hastening cross-bridge detachment [41]. Phosphorylation of cTnI and
304 cMyBPC accelerates relaxation either under β-adrenergic stimulation or increasing pacing
305 frequency which has been suggested to prevent diastolic dysfunction[42-44 45, 46].

306 In addition to the underlying effect of the elevated $SRCa^{2+}$ leak on the depressed
307 inotropic response of our HFpEF cardiomyocytes, an inability to properly cycle cross-bridges
308 might be also involved. cMyBPC directly promotes force generation by enhancing cross-bridge
309 binding and cooperative recruitment[47]. cMyBPC also acts as a brake on cross-bridge kinetics by
310 slowing down actin-myosin detachment[48, 49], an effect that is removed by phosphorylation of
311 cMyBPC [47, 50, 51]. MR-356 treatment prevented depressed phosphorylation of cMyBPC at serine
312 282 in HFpEF cardiomyocytes and might account, in part, for the preserved contractile reserve in
313 HFpEF cardiomyocytes treated with GHRH-A.

314 Among various synthetic GHRH agonists tested, MR-356 combines its high GHRH
315 activity and ventricular remodeling prevention in a rat model of acute myocardial infarction,
316 inducing the greatest reducing effect on infarct size[21]. At variance with those GHRH agonists
317 with high activation potency of GHRHR, but little or no myocardial repair capacity, downstream
318 activation of GHRHR by MR-356 might stimulate reparative pathways including adenylate
319 cyclase/PKA signaling. Likewise, MR-356 has been shown to promote survival of cardiac stem
320 cell and induce proliferation in vitro, possibly mediated by ERK1/2 and PI3K/AKT pathways[52].
321 JI-38, a GHRH-A comparable to MR-356 in terms of prevention of ventricular remodeling, has
322 been demonstrated to promote the up-regulation of the transcription factor GATA-4 and
323 proliferation within the myocardium[23]. A recent study using a model of pressure overload[26],
324 which exhibits characteristics of HFrEF, shows that the GHRH-A MR-409 attenuates remodeling
325 and improves myocardial function. These beneficial effects are consistent with previous
326 publications from our and other groups. However, while Gesmundo's work addresses a model
327 that has been studied for decades, transaortic constriction, in which several therapeutic strategies
328 have been confirmed as effective as they are in humans with HFrEF, our work focusses on a
329 highly relevant clinical problem with major unmet needs, the HFpEF syndrome. Our new results
330 show for first time the action of GHRH-As on the prevention and the reversal of the HFpEF

331 phenotype, especially diastolic dysfunction. Thus, based in the proven properties for cardiac
332 repair of GHRH-As and the robust and convincing data obtained in the present study, we
333 consider that GHRH-As are potentially useful for the management of HFpEF.

334 In summary, here we have shown that activation of GHRHR with a synthetic GHRH
335 agonist prevents the appearance of the HFpEF phenotype and reverses the signs of HFpEF once
336 established in mice, including dysfunctional diastolic relaxation in myocytes and intact animals
337 and myocardial remodeling. Increased SR Ca^{2+} leak associated with higher affinity of
338 myofilaments for Ca^{2+} and impaired cross-bridge cycling, underlie the dysfunctional contractile
339 response and lusitropy in these HFpEF cardiomyocytes, and may in part account for the
340 alterations in Ca^{2+} kinetics. Myofibrillar proteins appear to be a target for treatment with GHRH
341 agonists. Taken together these findings indicate that synthetic analogs of GHRH represent novel
342 therapeutic compounds for treating patients with the HFpEF syndrome.

343

344 **Methods.**

345 *Experimental design and animal model*

346 We used age matched (2-month old) CD1 mice (n=63, from Envigo). Mice were
347 implanted with a mini-osmotic pump (Alzet) to deliver Ang-II (0.2 mg/kg/day; Sigma-Aldrich
348 Co., Saint Louis, MO) for 4 weeks. Simultaneously, mice received daily injections of GHRH-
349 Agonist (GHRH-A [MR-356]: 200 μg/kg, n=23) or vehicle (DMSO+propylene-glycol, n=23)
350 during the same period of time. Unmanipulated (no mini-osmotic pump) age-matched CD1 mice
351 (n=17) were used as normal controls.

352 A separate group of CD1 mice (n=24, 2-month old) was implanted with the Alzet mini-
353 pumps containing Ang-II. After all mini-pumps content were delivered (4 weeks), the animals
354 were subjected to replacement of a mini-pumps for an additional 4-week Ang-II infusion. Upon
355 the second set of mini-pump implantation (day 29), the mice were randomized. Half of them
356 were daily injected with MR-356 and the remaining 12 mice received vehicle injections until the
357 day 56.

358 *Materials*

359 The GHRH-A, MR-356 ([N-Me-Tyr[1], Gln[8], Orn[12], Abu[15], Orn[21], Nle[27], Asp[28], Agm[29]]
360 hGH-RH(1-29)), was synthetized by solid phase methods and purified by HPLC in our
361 laboratories as described previously[21].

362 *Echocardiography*

363 Transthoracic echocardiography was performed as previously described with minor
364 modifications[53]. Briefly, mice were screened at baseline and 4 weeks following mini-osmotic
365 pump placement. All echocardiographic measurements were performed offline over 3 to 5 heart
366 beats.

367 *Speckle Tracking Echocardiography (STE)*

368 Strain analysis was conducted using speckle-tracking software, Vevostrain TM analysis
369 (Visual Sonics). Global longitudinal strain was calculated using B-mode cine images in the LV
370 parasternal long-axis view acquired at a high frame rate.

371 *Hemodynamic Measurements*

372 Hemodynamic studies were performed using a micro-tipped pressure-volume catheter
373 (SPR-839; Millar Instruments) as previously described with minor modifications. Briefly, the
374 catheter was inserted into the right carotid artery and advanced retrograde into the LV. Pressure-
375 volume loops were recorded at steady state, and during temporary inferior vena cava occlusion.
376 All analyses were performed using LabChart Pro version 8.1.5 software (ADInstruments). End-
377 diastolic pressure-volume pairs were plotted and then fitted by a linear regression. The reported
378 data representing the end-diastolic pressure-volume relationship (EDPVR) correspond to the
379 slope of the linear fitting: "stiffness coefficient" (mmHg/L).

380 *Cardiomyocyte Isolation*

381 Cardiac myocytes were isolated and prepared from hearts of mice by retrograde perfusion
382 through the aorta in a modified Langerdorf system with collagenase type 2 and protease type XIV
383 in an isolation solution (see the detailed procedure in the Supplemental Material online).
384 Cardiomyocytes were resuspended in Tyrode's buffer with 1.8 mmol/L $CaCl_2$, while a small
385 aliquot was kept in the presence of 10 mmol/L 2,3-butanedione monoxime (BDM) for cell length
386 and width measurement.

387 *Intracellular Calcium and Sarcomere Length Measurement*

388 Intracellular Ca^{2+} was measured using the Ca^{2+}-sensitive dye Fura-2 and a dual-excitation
389 (340/380 nm) spectrofluorometer (IonOptix LLC, Milton, MA, USA) in cardiomyocytes electric-
390 field stimulated at 1, 2 and 4 Hz. $[Ca^{2+}]_i$ was calculated as described previously[54]. $\Delta[Ca^{+2}]_i$
391 amplitude was considered as: peak $[Ca^{+2}]_i$ – resting $[Ca^{+2}]_i$(see detailed methodology in the online
392 Supplemental Material). Simultaneously, sarcomere length (SL) was recorded with an IonOptix
393 iCCD camera. Change in average SL was determined by Fast Fourier Transform analysis of the
394 Z-line density trace to the frequency domain, and SL shortening (SLS) was calculated as:
395 $SLS(\%)=100\times(resting\ SL-peak\ SL)/resting\ SL$.

396 *Hysteresis Sarcomere Shortening-Calcium Loop Analysis*

397 The hysteresis loops were obtained by plotting sarcomere length versus calcium
398 concentration of cardiomyocytes paced at 4 Hz. Two of the three main segments of such loops
399 were analyzed for this work: the "force-activation" and the "relaxation" phases[34, 55] (see detailed
400 explanation in the online Supplemental Material). The analyses of both, relaxation and force-
401 activation phases were performed by GraphPad Prism version 6.07 (San Diego, CA USA).

402 *SR Ca^{2+} Leak and SR Ca^{2+} Load Measurement*

403 SR Ca^{2+} leakage was assessed with 1 mmol/L tetracaine (Sigma-Aldrich) using a modified
404 protocol from the one described by Shannon *et al*[56]. Briefly, the observed decrease in the Fura-2
405 ratio in presence of tetracaine compared to the not-tetracaine treated condition was considered the
406 Ca^{2+} leak for a particular myocyte (detailed methodology is provided in the online Supplemental
407 Material). After tetracaine wash out, SR Ca^{2+} content was assessed on the same cell by a 20
408 mmol/L caffeine challenge. SR Ca^{2+} contents were calculated considering that SR represents 3.5%
409 and cytosol 65% of the myocyte volume. Ca^{2+} leak-SR $[Ca^{2+}]$ pairs were grouped by similar SR
410 $[Ca^{2+}]$ load, plotted and fitted by an exponential growth function using the Graph Pad Prism
411 software (version 6.07). Measurements were carried out at 37°C.

412 *Western Blot Immunoanalysis*

413 *Isolated cardiomyocytes:* Frozen cardiomyocytes were lysed in ice-cold RIPA buffer with
414 proteinase inhibitors (cOmplete protease inhibitor cocktail; Roche), sonicated and then
415 centrifuged at 12500 RPM for 15 minutes at 4°C.

416 *Hearts:* Frozen cardiac tissues were homogenized using a Pyrex glass-glass homogenizer
417 on liquid nitrogen using a urea-based lysing buffer. The samples were then centrifuged.

418 Supernatants from either procedure were collected and sampled for protein concentration.
419 Samples were electrophoresed and transferred to PVDF or nitrocellulose membranes (Bio-Rad
420 Laboratories). Detection of proteins was performed by immunoblotting using the adequate
421 antibodies as indicated (please, see detailed information in the Supplemental Material online).

422 *Quantitative RT-PCR*

423 Total RNA was isolated from cardiomyocytes using RNAeasy mini kit (Qiagen, Hilden,
424 Germany). RNA (1 μg) was reverse-transcribed according to instructions utilizing a cDNA
425 Synthesis kit (Applied Biosystems, Foster City, CA). Using Taqman® Universal Master Mix
426 (Applied Biosystems, Foster City, CA) in a Bio-Rad CFX96™ Real-Time PCR system (Bio-Rad
427 Laboratories, Hercules, CA, USA), qPCR was performed. All samples were run in duplicates and
428 normalized to 18S Taqman gene-expression as follows: ATP2a2: Mm01201431_m1; RYR2
429 Mm00465877_m1, TNNi1: Mm00502426_m1; TNNi3: Mm00437164_m1; MHY6:
430 Mm00440359_m1; MHY7: Mm00600555_m1and 18S Mm03928990_g1. The change in mRNA
431 expression was calculated compared to the change in normalized 18S, and values were expressed
432 as 2ΔCt.

433 Statistical Analysis

434 Data are reported as mean ± standard error of the mean (SEM). Statistical significance
435 between three groups was determined by one-way ANOVA, or two-way ANOVA followed by
436 Sidak's or Bonferonni's post hoc tests, as appropriate. For comparisons of two groups, Student's
437 t-test two-tailed was used. Analyses were performed using GraphPad Prism version 8.3.0. The
438 null hypothesis was rejected at $p<0.05$.

439 *Study approval*

440 All protocols and experimental procedures were approved by the University of Miami
441 Animal Care and Use Committee following the Guide for the Care and Use of Laboratory
442 Animals (NIH Publication No. 85-234, revised 2011).

443

References

1. Berlot, B., Bucciarelli-Ducci, C., Palazzuoli, A. & Marino, P. Myocardial phenotypes and dysfunction in HFpEF and HFrEF assessed by echocardiography and cardiac magnetic resonance. *Heart Fail Rev* (2019).
2. Lewis, G.A. et al. Biological Phenotypes of Heart Failure With Preserved Ejection Fraction. *J Am Coll Cardiol* **70**, 2186-2200 (2017).
3. Pieske, B. et al. How to diagnose heart failure with preserved ejection fraction: the HFA-PEFF diagnostic algorithm: a consensus recommendation from the Heart Failure Association (HFA) of the European Society of Cardiology (ESC). *Eur Heart J* **40**, 3297-3317 (2019).
4. Owan, T.E. et al. Trends in prevalence and outcome of heart failure with preserved ejection fraction. *N Engl J Med* **355**, 251-259 (2006).
5. Oktay, A.A., Rich, J.D. & Shah, S.J. The emerging epidemic of heart failure with preserved ejection fraction. *Curr Heart Fail Rep* **10**, 401-410 (2013).
6. Silverman, D.N. et al. Association of beta-Blocker Use With Heart Failure Hospitalizations and Cardiovascular Disease Mortality Among Patients With Heart Failure With a Preserved Ejection Fraction: A Secondary Analysis of the TOPCAT Trial. *JAMA Netw Open* **2**, e1916598 (2019).
7. Pitt, B. et al. Spironolactone for heart failure with preserved ejection fraction. *N Engl J Med* **370**, 1383-1392 (2014).
8. Solomon, S.D. et al. Angiotensin-Neprilysin Inhibition in Heart Failure with Preserved Ejection Fraction. *N Engl J Med* **381**, 1609-1620 (2019).
9. O'Connor, C.M. & deFilippi, C. PARAGON-HF - Why We Do Randomized, Controlled Clinical Trials. *N Engl J Med* **381**, 1675-1676 (2019).
10. Takada, T. et al. Impact of elevated heart rate on clinical outcomes in patients with heart failure with reduced and preserved ejection fraction: a report from the CHART-2 Study. *Eur J Heart Fail* **16**, 309-316 (2014).
11. Melenovsky, V. et al. Cardiovascular features of heart failure with preserved ejection fraction versus nonfailing hypertensive left ventricular hypertrophy in the urban Baltimore community: the role of atrial remodeling/dysfunction. *J Am Coll Cardiol* **49**, 198-207 (2007).
12. Yang, J.H. et al. Endothelium-dependent and independent coronary microvascular dysfunction in patients with heart failure with preserved ejection fraction. *Eur J Heart Fail* (2019).
13. Shah, S.J. et al. Phenotype-Specific Treatment of Heart Failure With Preserved Ejection Fraction: A Multiorgan Roadmap. *Circulation* **134**, 73-90 (2016).
14. Schiattarella, G.G. et al. Nitrosative stress drives heart failure with preserved ejection fraction. *Nature* **568**, 351-356 (2019).
15. Obokata, M. et al. The neurohormonal basis of pulmonary hypertension in heart failure with preserved ejection fraction. *Eur Heart J* **40**, 3707-3717 (2019).
16. Kjeldsen, S.E. et al. Medical Therapies for Heart Failure With Preserved Ejection Fraction. *Hypertension* **75**, 23-32 (2020).
17. Tarone, G. et al. Targeting myocardial remodelling to develop novel therapies for heart failure: a position paper from the Working Group on Myocardial Function of the European Society of Cardiology. *Eur J Heart Fail* **16**, 494-508 (2014).
18. Redfield, M.M. et al. Isosorbide Mononitrate in Heart Failure with Preserved Ejection Fraction. *N Engl J Med* **373**, 2314-2324 (2015).
19. Banerjee, P. Heart failure with preserved ejection fraction: A clinical crisis. *Int J Cardiol* **204**, 198-199 (2016).
20. Fernandez-Ruiz, I. The search for an effective HFpEF treatment continues. *Nat Rev Cardiol* **16**, 647 (2019).
21. Cai, R. et al. Synthesis of new potent agonistic analogs of growth hormone-releasing hormone (GHRH) and evaluation of their endocrine and cardiac activities. *Peptides* **52**, 104-112 (2014).

494 22. Granata, R. et al. Growth hormone-releasing hormone promotes survival of cardiac myocytes in
495 vitro and protects against ischaemia-reperfusion injury in rat heart. *Cardiovasc Res* **83**, 303-312
496 (2009).
497 23. Kanashiro-Takeuchi, R.M. et al. Activation of growth hormone releasing hormone (GHRH)
498 receptor stimulates cardiac reverse remodeling after myocardial infarction (MI). *Proc Natl Acad*
499 *Sci U S A* **109**, 559-563 (2012).
500 24. Kanashiro-Takeuchi, R.M. et al. Cardioprotective effects of growth hormone-releasing hormone
501 agonist after myocardial infarction. *Proc Natl Acad Sci U S A* **107**, 2604-2609 (2010).
502 25. Bagno, L.L. et al. Growth hormone-releasing hormone agonists reduce myocardial infarct scar in
503 swine with subacute ischemic cardiomyopathy. *J Am Heart Assoc* **4** (2015).
504 26. Gesmundo, I. et al. Growth hormone-releasing hormone attenuates cardiac hypertrophy and
505 improves heart function in pressure overload-induced heart failure. *Proc Natl Acad Sci U S A*
506 **114**, 12033-12038 (2017).
507 27. Matsubara, S., Sato, M., Mizobuchi, M., Niimi, M. & Takahara, J. Differential gene expression of
508 growth hormone (GH)-releasing hormone (GRH) and GRH receptor in various rat tissues.
509 *Endocrinology* **136**, 4147-4150 (1995).
510 28. Conceicao, G., Heinonen, I., Lourenco, A.P., Duncker, D.J. & Falcao-Pires, I. Animal models of
511 heart failure with preserved ejection fraction. *Neth Heart J* **24**, 275-286 (2016).
512 29. Primessnig, U. et al. Novel pathomechanisms of cardiomyocyte dysfunction in a model of heart
513 failure with preserved ejection fraction. *Eur J Heart Fail* **18**, 987-997 (2016).
514 30. Olver, T.D. et al. Western Diet-Fed, Aortic-Banded Ossabaw Swine: A Preclinical Model of
515 Cardio-Metabolic Heart Failure. *JACC Basic Transl Sci* **4**, 404-421 (2019).
516 31. Matyas, C. et al. Prevention of the development of heart failure with preserved ejection fraction
517 by the phosphodiesterase-5A inhibitor vardenafil in rats with type 2 diabetes. *Eur J Heart Fail*
518 **19**, 326-336 (2017).
519 32. Regan, J.A. et al. A mouse model of heart failure with preserved ejection fraction due to chronic
520 infusion of a low subpressor dose of angiotensin II. *Am J Physiol Heart Circ Physiol* **309**, H771-
521 778 (2015).
522 33. Wang, J., Khoury, D.S., Yue, Y., Torre-Amione, G. & Nagueh, S.F. Preserved left ventricular
523 twist and circumferential deformation, but depressed longitudinal and radial deformation in
524 patients with diastolic heart failure. *Eur Heart J* **29**, 1283-1289 (2008).
525 34. Tong, C.W., Gaffin, R.D., Zawieja, D.C. & Muthuchamy, M. Roles of phosphorylation of myosin
526 binding protein-C and troponin I in mouse cardiac muscle twitch dynamics. *J Physiol* **558**, 927-
527 941 (2004).
528 35. Tong, C.W., Nair, N.A., Doersch, K.M., Liu, Y. & Rosas, P.C. Cardiac myosin-binding protein-C
529 is a critical mediator of diastolic function. *Pflugers Arch* **466**, 451-457 (2014).
530 36. Tadic, M., Cuspidi, C., Frydas, A. & Grassi, G. The role of arterial hypertension in development
531 heart failure with preserved ejection fraction: just a risk factor or something more? *Heart Fail*
532 *Rev* **23**, 631-639 (2018).
533 37. Shannon, T.R., Ginsburg, K.S. & Bers, D.M. Reverse mode of the sarcoplasmic reticulum
534 calcium pump and load-dependent cytosolic calcium decline in voltage-clamped cardiac
535 ventricular myocytes. *Biophys J* **78**, 322-333 (2000).
536 38. Diaz, M.E., Trafford, A.W. & Eisner, D.A. The effects of exogenous calcium buffers on the
537 systolic calcium transient in rat ventricular myocytes. *Biophys J* **80**, 1915-1925 (2001).
538 39. Kataoka, A., Hemmer, C. & Chase, P.B. Computational simulation of hypertrophic
539 cardiomyopathy mutations in troponin I: influence of increased myofilament calcium sensitivity
540 on isometric force, ATPase and [Ca2+]i. *J Biomech* **40**, 2044-2052 (2007).
541 40. Perez, N.G. et al. A low dose of angiotensin II increases inotropism through activation of reverse
542 Na(+)/Ca(2+) exchange by endothelin release. *Cardiovasc Res* **60**, 589-597 (2003).
543 41. Baker, A.J. & Weiner, M.W. Force decline during muscle relaxation promotes calcium release to
544 the cytosol. *Am J Physiol* **273**, C85-91 (1997).

545 42. Colson, B.A. et al. Myosin binding protein-C phosphorylation is the principal mediator of protein
546 kinase A effects on thick filament structure in myocardium. *J Mol Cell Cardiol* **53**, 609-616
547 (2012).
548 43. Varian, K.D. & Janssen, P.M. Frequency-dependent acceleration of relaxation involves decreased
549 myofilament calcium sensitivity. *Am J Physiol Heart Circ Physiol* **292**, H2212-2219 (2007).
550 44. Varian, K.D. et al. Impairment of diastolic function by lack of frequency-dependent myofilament
551 desensitization rabbit right ventricular hypertrophy. *Circ Heart Fail* **2**, 472-481 (2009).
552 45. Dweck, D. et al. Long term ablation of protein kinase A (PKA)-mediated cardiac troponin I
553 phosphorylation leads to excitation-contraction uncoupling and diastolic dysfunction in a knock-
554 in mouse model of hypertrophic cardiomyopathy. *J Biol Chem* **289**, 23097-23111 (2014).
555 46. Takimoto, E. et al. Frequency- and afterload-dependent cardiac modulation in vivo by troponin I
556 with constitutively active protein kinase A phosphorylation sites. *Circ Res* **94**, 496-504 (2004).
557 47. Coulton, A.T. & Stelzer, J.E. Cardiac myosin binding protein C and its phosphorylation regulate
558 multiple steps in the cross-bridge cycle of muscle contraction. *Biochemistry* **51**, 3292-3301
559 (2012).
560 48. Razumova, M.V., Bezold, K.L., Tu, A.Y., Regnier, M. & Harris, S.P. Contribution of the myosin
561 binding protein C motif to functional effects in permeabilized rat trabeculae. *J Gen Physiol* **132**,
562 575-585 (2008).
563 49. Saber, W., Begin, K.J., Warshaw, D.M. & VanBuren, P. Cardiac myosin binding protein-C
564 modulates actomyosin binding and kinetics in the in vitro motility assay. *J Mol Cell Cardiol* **44**,
565 1053-1061 (2008).
566 50. Shaffer, J.F., Kensler, R.W. & Harris, S.P. The myosin-binding protein C motif binds to F-actin
567 in a phosphorylation-sensitive manner. *J Biol Chem* **284**, 12318-12327 (2009).
568 51. Sadayappan, S. et al. A critical function for Ser-282 in cardiac Myosin binding protein-C
569 phosphorylation and cardiac function. *Circ Res* **109**, 141-150 (2011).
570 52. Florea, V. et al. Agonists of growth hormone-releasing hormone stimulate self-renewal of cardiac
571 stem cells and promote their survival. *Proc Natl Acad Sci U S A* **111**, 17260-17265 (2014).
572 53. Yuan, C.C. et al. Constitutive phosphorylation of cardiac myosin regulatory light chain prevents
573 development of hypertrophic cardiomyopathy in mice. *Proc Natl Acad Sci U S A* **112**, E4138-
574 4146 (2015).
575 54. Dulce, R.A. et al. Hydralazine and organic nitrates restore impaired excitation-contraction
576 coupling by reducing calcium leak associated with nitroso-redox imbalance. *J Biol Chem* **288**,
577 6522-6533 (2013).
578 55. Ramirez-Correa, G.A., Cortassa, S., Stanley, B., Gao, W.D. & Murphy, A.M. Calcium sensitivity,
579 force frequency relationship and cardiac troponin I: critical role of PKA and PKC
580 phosphorylation sites. *J Mol Cell Cardiol* **48**, 943-953 (2010).
581 56. Shannon, T.R., Ginsburg, K.S. & Bers, D.M. Quantitative assessment of the SR Ca2+ leak-load
582 relationship. *Circ Res* **91**, 594-600 (2002).

583

584 **Acknowledgments**

585 **Sources of funding:** Study was supported by NIH, grants 1R01 HL13735 and 1R01 HL107110
586 to JMH. JMH is also supported by NIH grants 5UM1 HL113460, 1R01 HL134558, 5R01
587 CA136387 and The Starr Foundation. São Paulo Research Foundation (FAPESP) grant#
588 2016/01044-0 (to AGS).

589 **Author contributions:** RAD was involved in designing research studies, and conducted
590 experiments, acquiring data, analyzing data, discussion and interpretation of results, and writing
591 the manuscript. RMKT, main responsible for designing research studies, she also conducted
592 experiments, acquiring and analyzing data, and discussing results. LMT conducted experiments,
593 acquired and analyzed data. AGS conducted experiments. SK analyzed and interpreted
594 echocardiographic measurements. WB participated in discussing results, writing and correction
595 of the manuscript. MSSRZ analyzed echocardiographic measurements. RC synthesized reagents.
596 AVS provided reagents and contributed to writing of the manuscript. JMH conceived the project,
597 participated in data and results interpretation, provided scientific and financial support for the
598 project, and contributed to writing of the manuscript.

599 **Competing interests:** Dr. Joshua Hare owned equity in Biscayne Pharmaceuticals, licensee of
600 intellectual property used in this study. Biscayne Pharmaceuticals did not provide funding for
601 this study. Dr. Joshua Hare is the Chief Scientific Officer, a compensated consultant and
602 advisory board member for Longeveron and holds equity in Longeveron. Dr. Hare is also the co-
603 inventor of intellectual property licensed to Longeveron. All other authors have declared that no
604 conflict of interest exists.

605 **Materials & Correspondence:** Additional information from the study is available and should be
606 requested to the corresponding author Dr. Joshua M. Hare: jhare@med.miami.edu

607

608 **Tables:**

609 - Table 1: Hemodynamic assessments on 4-week Ang-II infusion model

	Control (N=8)	Ang-II (N=9)	Ang-II+MR-356 (N=9)
HR (1/min)	535.9±11.7	543.9±7.2	523.5±14.2
EF (%)	51.0±4.0	55.7±5.8	59.6±2.9
Tau (1/sec)	5.21±0.33	7.12±0.57*	5.91±0.27†
dP/dt_{max} (mmHg/sec)	7328±346	6866±519	7433±476
dP/dt_{min} (mmHg/sec)	-5494±353	-4897±451	-7013±580*†
Ea (mmHg/μL)	1.65±0.25	1.95±0.29	1.83±0.13
LVEDP (mmHg)	4.13±0.89	6.46±0.38*	5.87±0.91
ESPVR (mmHg/μL)	2.71±0.28	1.57±0.19*	1.96±0.37*
EDPVR (mmHg/μL) [linear]	0.068±0.004	0.091±0.009*	0.059±0.004†
PRSW (mmHg/μL)	74.5±3.1	63.2±3.9	62.4±5.4
dP/dt_{max}-EDV (mmHg/μL.sec)	110.7±13.9	99.0±6.3	91.1±9.6
Systolic ABP (mmHg)	79.7±2.2	103.0±4.7*	88.5±4.6†
Diastolic ABP (mmHg)	54.7±2.7	75.5±3.7*	64.4±4.2

610

611 **Table 1:** All values represent mean±SEM. HR, heart rate; EF, ejection fraction; Tau, relaxation
612 constant; dP/dt_{max}, maximal contraction rate; dP/dt_{min}, maximal relaxation rate; Ea, arterial
613 elastance; LVEDP, left ventricular end-diastolic pressure; ESPVR, end-systolic pressure-volume
614 relationship; EDPVR, slope of the end-diastolic pressure-volume relationship; PRSW, Preload
615 recruitable stroke work; dP/dt_{max}-EDV, maximal contraction rate-end diastolic volume
616 relationship. ABP, arterial blood pressure. * $p<0.05$ vs. control; † $p<0.05$ Ang-II+MR-356 vs.
617 Ang-II, one-way ANOVA. N represents number of studied animals.

618 **Figures:**

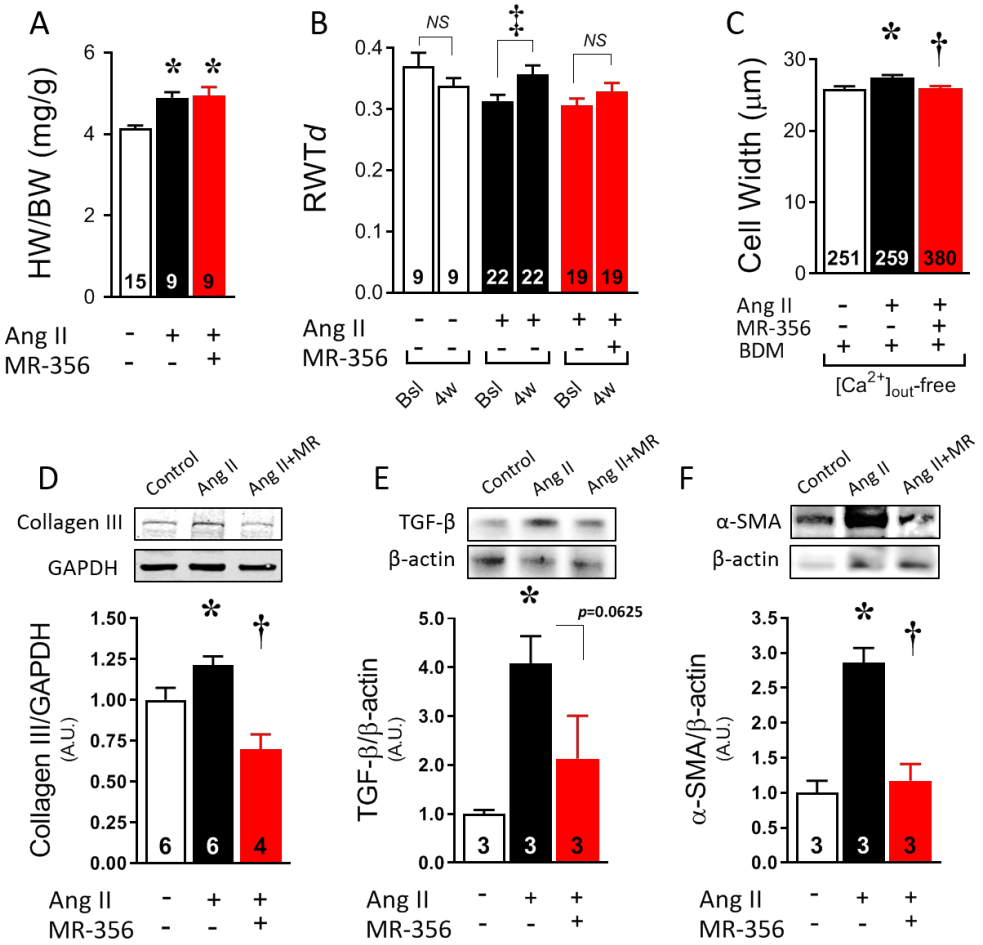

619

620 **Figure 1: Biometric, echocardiographic, cellular and molecular characterization of the**
621 **HFpEF model. GHRH-A MR-356 prevents cardiomyocyte growth and fibrosis.** (A) Heart size
622 normalized to body weight. (B) Relative wall thickness in diastole (RWTd) in different groups (‡
623 $p<0.05$ 4-week vs. baseline within groups; two-way ANOVA). (C) Width of isolated
624 cardiomyocytes from control (N=4), Ang-II-treated (N=5) and Ang-II+MR-356-treated (N=5)
625 mice. (D) Collagen III protein expression. Top, representative images of western blots. Bottom,
626 bar graph showing average results. (E) Transforming growth factor-β (TGF-β) and (F) α-smooth
627 muscle actin (α-SMA) protein expression in heart homogenates. *$p<0.05$ in Ang II vs. control and
628 † $p<0.05$ in Ang II+MR-356-treated vs. Ang II; One-way ANOVA. Numbers on bottom of bars
629 correspond to studied animals in panels A-B, while they indicate number of cells in panel C, or
630 tissue samples in panels D-F.

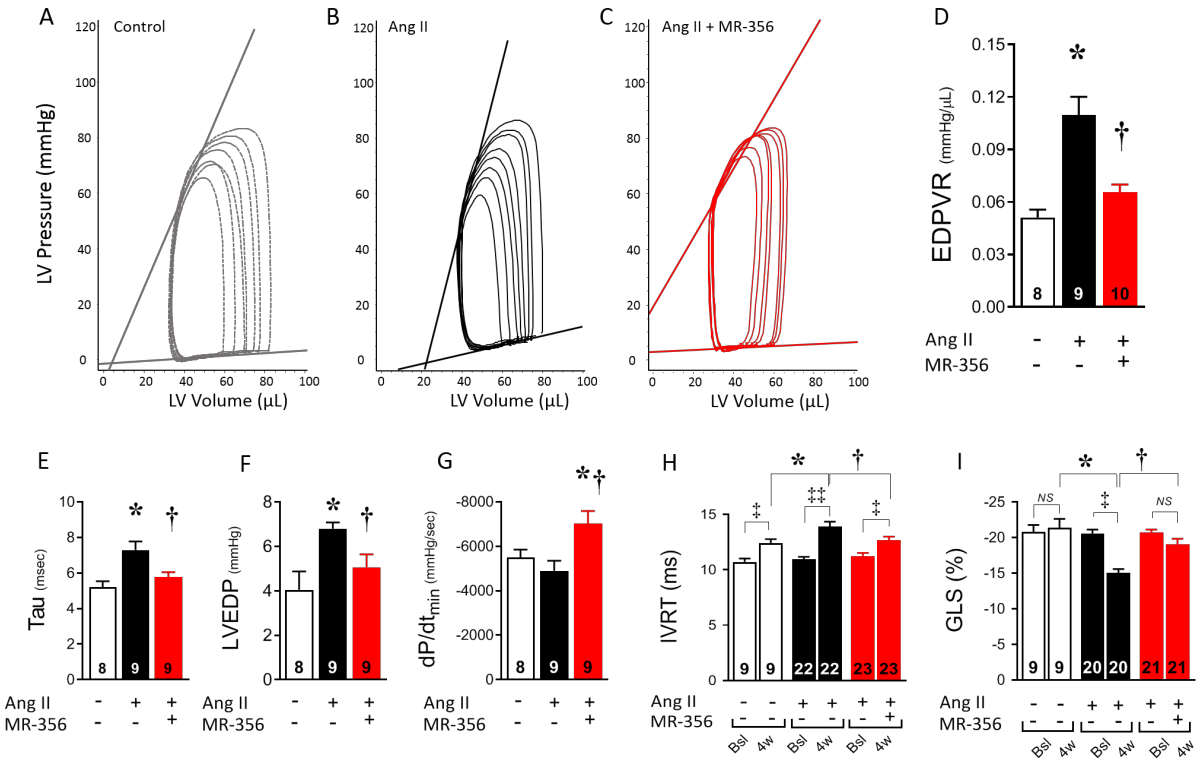

Figure 2: Effects of the GHRH-A MR-356 on diastolic dysfunction in the heart of Ang-II-induced HFpEF mice. (A) Representative pressure-volume (P-V) loops showing the linear regression for end-systolic pressure-volume relationship (ESPVR) and end-diastolic pressure-volume relationship (EDPVR) in a control mouse, or (B) Ang-II-treated mouse, or (C) Ang-II+MR-356 mouse. (D) Averaged slopes from the EDPVR linear fitting. (E) Hemodynamic assessment of the relaxation time constant (tau) at 4-week time point. (F) Left ventricular end-diastolic pressure (LVEDP). (G) Maximal rate of pressure decline (dP/dt_{min}). (H) Isovolumic relaxation time (IVRT) as measured by transthoracic echocardiography at baseline or after 4-week treatment. (I) Global longitudinal strain (GLS) analysis of the left ventricle assessed in same conditions. GLS represents the function of sub-endocardial longitudinal myocardial fibers that are more sensitive to reduced coronary perfusion and increased wall stress. Moreover, GLS reflects changes in the myocardial interstitium including the extent of myocardial fibrosis. ‡ $p<0.05$ at 4-week vs. baseline; ‡‡ $p<0.001$ at 4-week vs. baseline, two-way ANOVA. *$p<0.05$ vs. control; † $p<0.05$ in Ang-II+MR-356-treated vs. Ang-II; one or two-way ANOVA. Numbers on bottom of bars indicate number of analyzed animals.

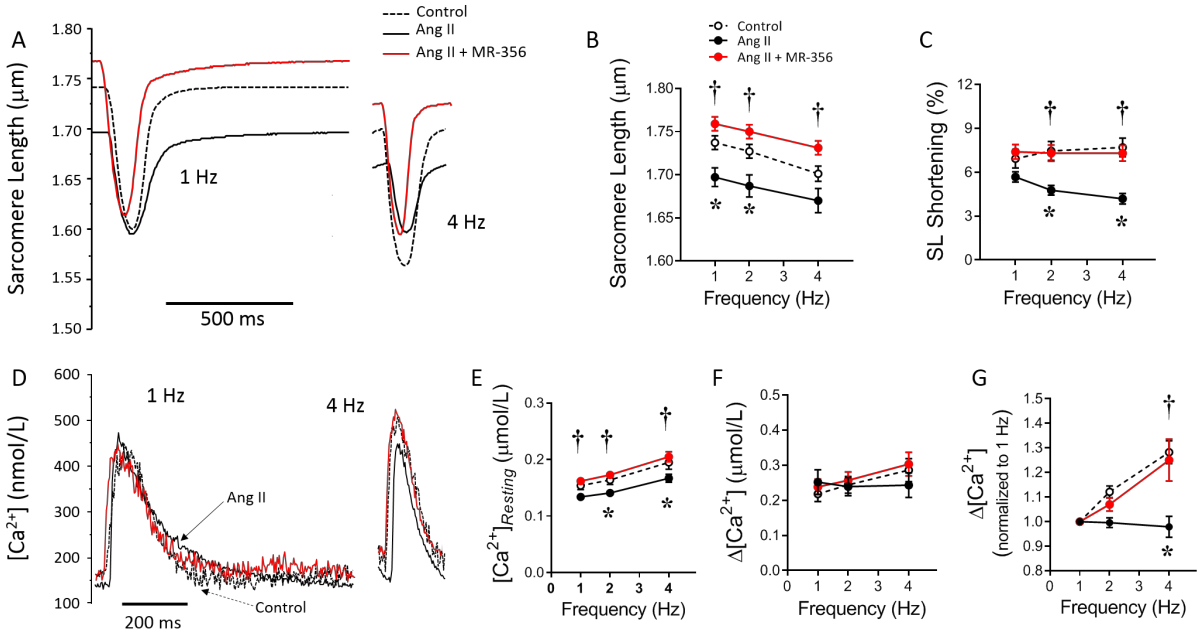

Figure 3: Sarcomere and contractile dysfunction in the HFpEF model is prevented by co-treatment with GHRH-A MR-356. (A) Representative traces of sarcomere twitches of cardiomyocytes paced at 1 and 4 Hz obtained from CD1 control mice (N=4, 30 cells) or mice which underwent either Ang-II infusion (N=5, 41 cells) or Ang-II+MR-356 treatment (N=5, 38 cells). (B) Resting sarcomere length in cardiomyocytes from each group at different pacing rates. (C) Sarcomere shortening in response to pacing. (D) Representative traces of intracellular $[Ca^{2+}]$ in cardiomyocytes electric field-stimulated in same conditions as above. (E) $\Delta[Ca^{2+}]$ transient amplitude in response to pacing. (F) $\Delta[Ca^{2+}]$ transient-frequency relationship normalized respect to 1 Hz. (G) Diastolic $[Ca^{2+}]$ in response to increasing frequency of stimulation. From each mouse, a total of 5 to 9 cells were studied. *$p<0.05$ in Ang-II vs. control and † $p<0.05$ in Ang-II+MR-356-treated vs. Ang-II; two-way ANOVA.

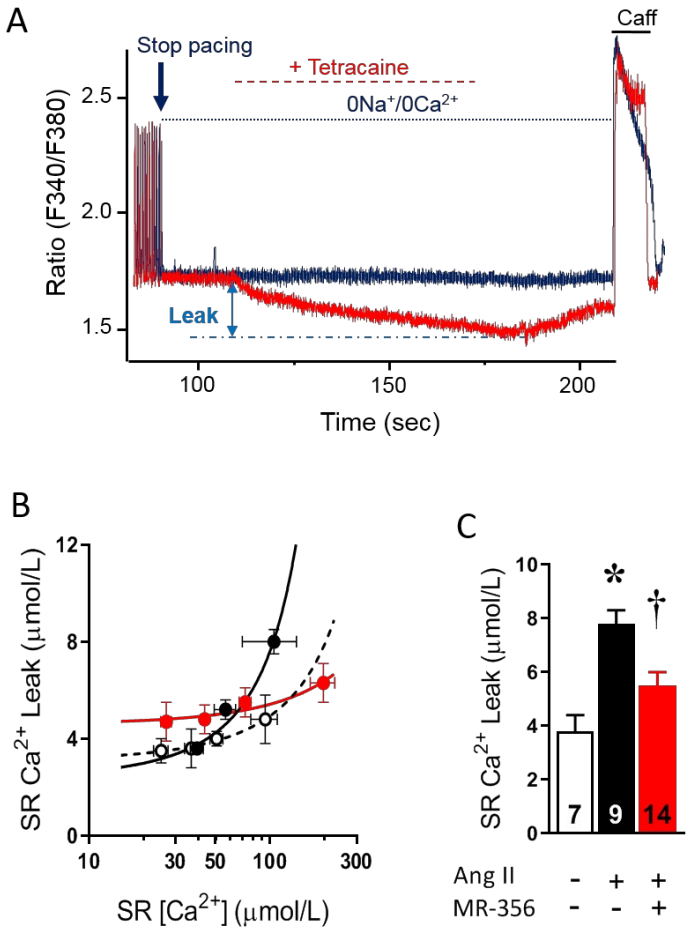

Figure 4: Increased SR Ca^{2+} leak in HFpEF cardiomyocytes is prevented by treatment with the GHRH-A MR-356. (A) Representative traces of intracellular [Ca^{2+}] in cardiomyocytes illustrating the method for measuring SR Ca^{2+} leak using tetracaine. Blue trace corresponds to Ca^{2+} from a cardiomyocyte not exposed to tetracaine, while red trace is the Ca^{2+} from the same cardiomyocyte that was treated 70 seconds with tetracaine. (B) SR Ca^{2+} leak-load relationship in cardiomyocytes from control untreated (n=31 cells), Ang-II-treated (n=38 cells) or Ang-II+MR-356-treated (n=35 cells) CD1 mice. (C) Average SR Ca^{2+} leak in cardiomyocytes from all groups at matched SR Ca^{2+} load=99.1 µmol/L. *p<0.05 in Ang-II vs. control and † p<0.05 in Ang-II-treated vs. Ang-II+MR-356-treated; one or two-way ANOVA as appropriate. Numbers on bottom of bars indicate number of analyzed cells.

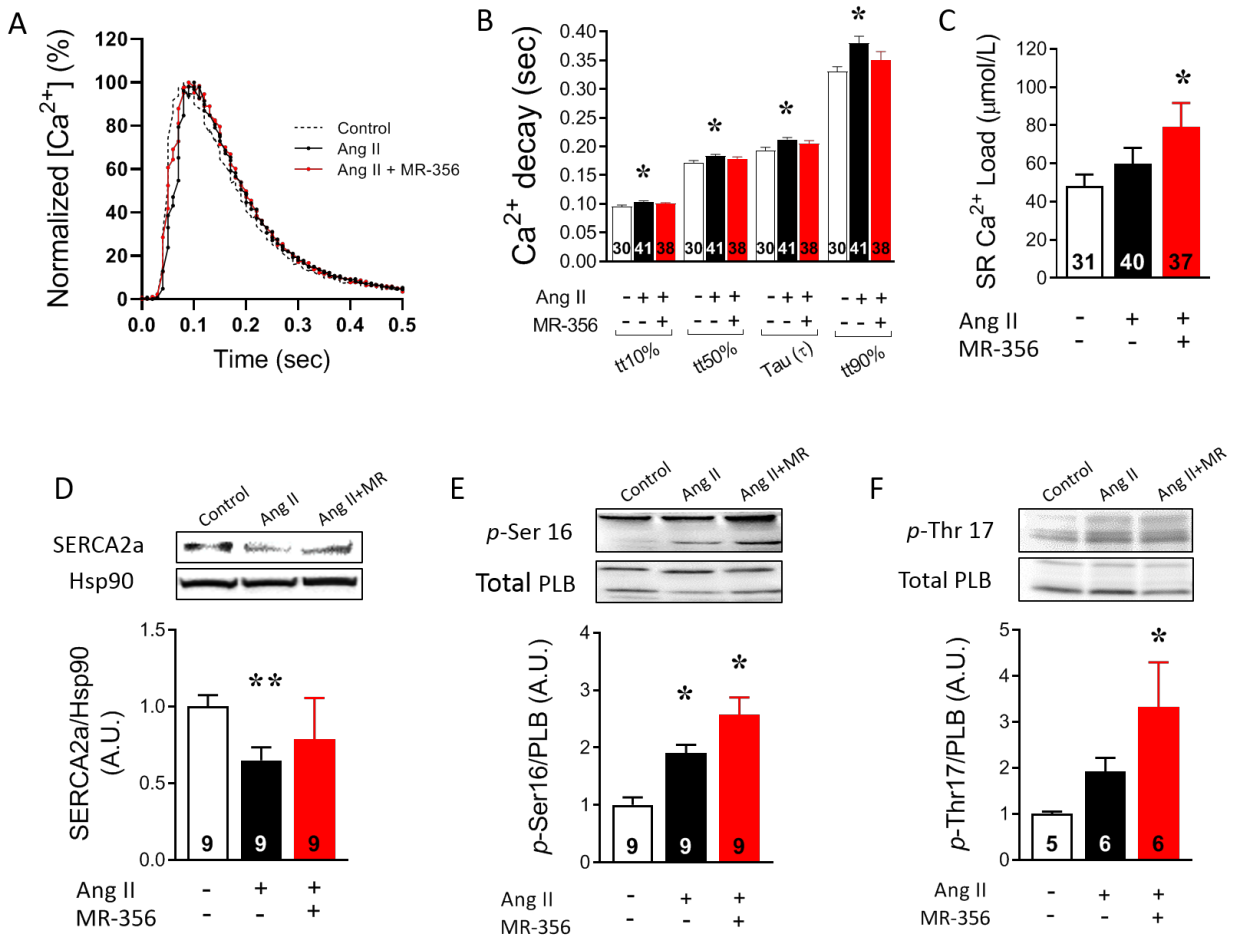

Figure 5: **Ca^{2+} decay is delayed in cardiomyocytes from the Ang-II-induced HFpEF model but preserved by treatment with the GHRH-A MR-356.** (A) Normalized Ca^{2+} transient reconstructed by using average dynamic parameters from control untreated, Ang-II-treated or Ang-II+MR-356-treated cardiomyocytes paced at 1 Hz. (B) Average times to different degrees of the Ca^{2+} peak decline: time to 10% (tt10%), time to 50% (tt50%), decay time constant (τ) and time to 90% (tt90%). (C) SR Ca^{2+} content in cardiomyocytes paced at 1 Hz from each group. Numbers on bottom of bars on panels B and C indicate number of analyzed cells. (D) SERCA2a protein expression; top, representative immunoblotting image with Hsp90 as loading control and bottom, average values of SERCA2a expression. (E) PLB phosphorylation at serine 16. (F) Phosphorylation of PLB at threonine 17. Top, representative images and bottom, average values. Numbers on bottom of bars on panels D, E and F indicate number of analyzed samples. *p<0.05 or **p<0.01 vs. control, † p<0.05 vs. Ang-II-treated; one-way ANOVA.

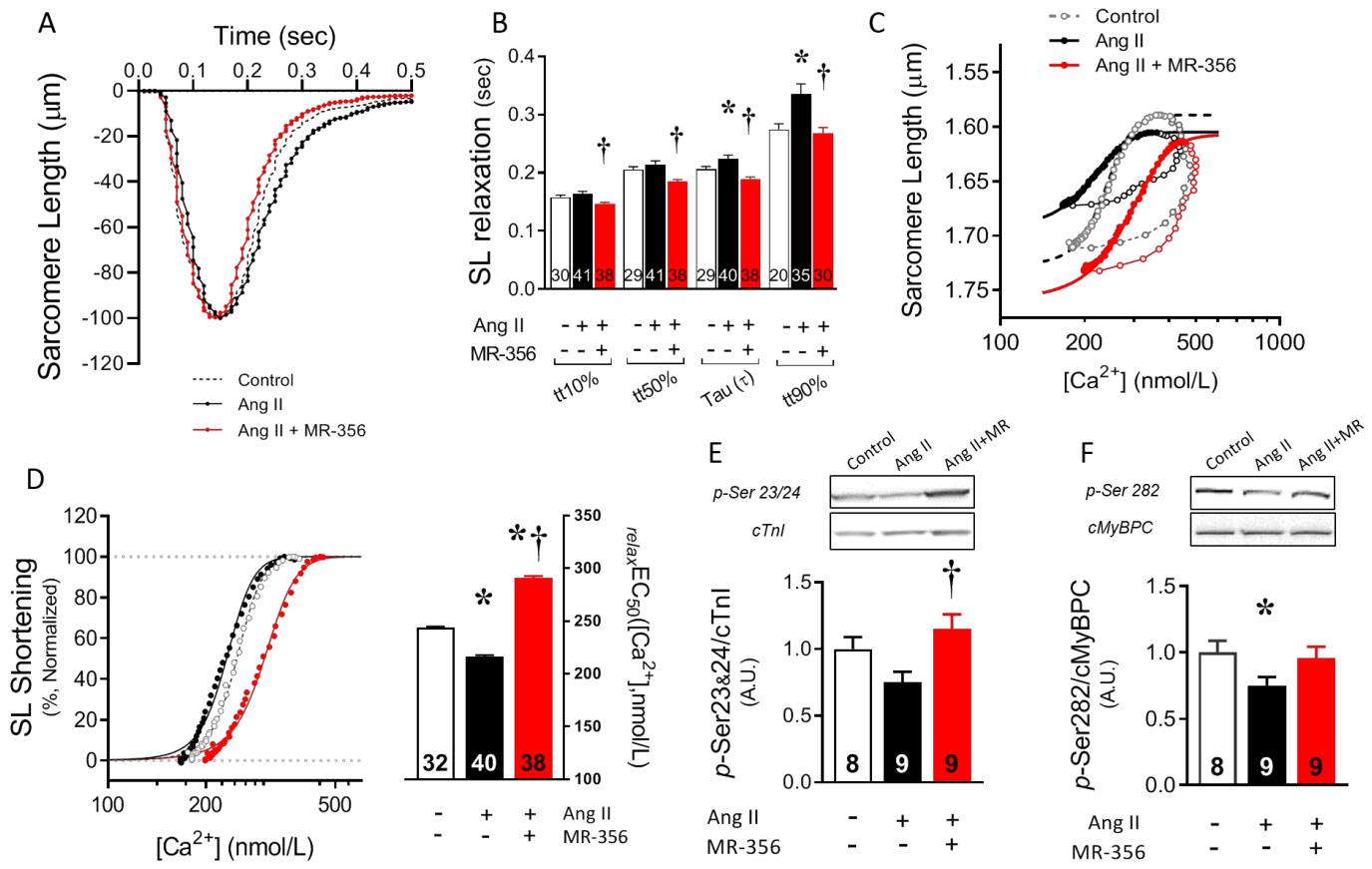

Figure 6: **Impairment in sarcomere relaxation due to myofilaments sensitization in HFpEF cardiomyocytes is prevented by treatment with the GHRH-A MR-356.** (A) Normalized sarcomere contraction re-constructed by using average SL at 1Hz from control untreated, Ang- II-treated or Ang-II+MR-356-treated cardiomyocytes. (B) Average times to different degrees of the relaxation: tt10%, tt50%, tau (τ) and tt90%. (C) SL-[Ca^{2+}] hysteresis loops in control, Ang-II- or Ang-II+MR-356-treated cardiomyocytes with overlapped sigmoidal fitting of the relaxation phases. (D) Normalized relaxation phase of SL-[Ca^{2+}] loops (left) and averaged effective [Ca^{2+}] of the relaxation phase ($_{relax}EC_{50}$s, right). Numbers on bottom of bars on panel D indicate number of analyzed cells from 4-5 hearts. (E) Phosphorylation of cTnI at serine 23/24 and total protein expression by western blot. (F) Phosphorylation of cMyBPC at serine 282 and total protein expression. Top, representative images; bottom, average values. Numbers on bottom of bars on panels E and F indicate number of analyzed samples. *p<0.05 vs. control, † p<0.05 vs. Ang-II + MR-356-treated; one-way ANOVA.

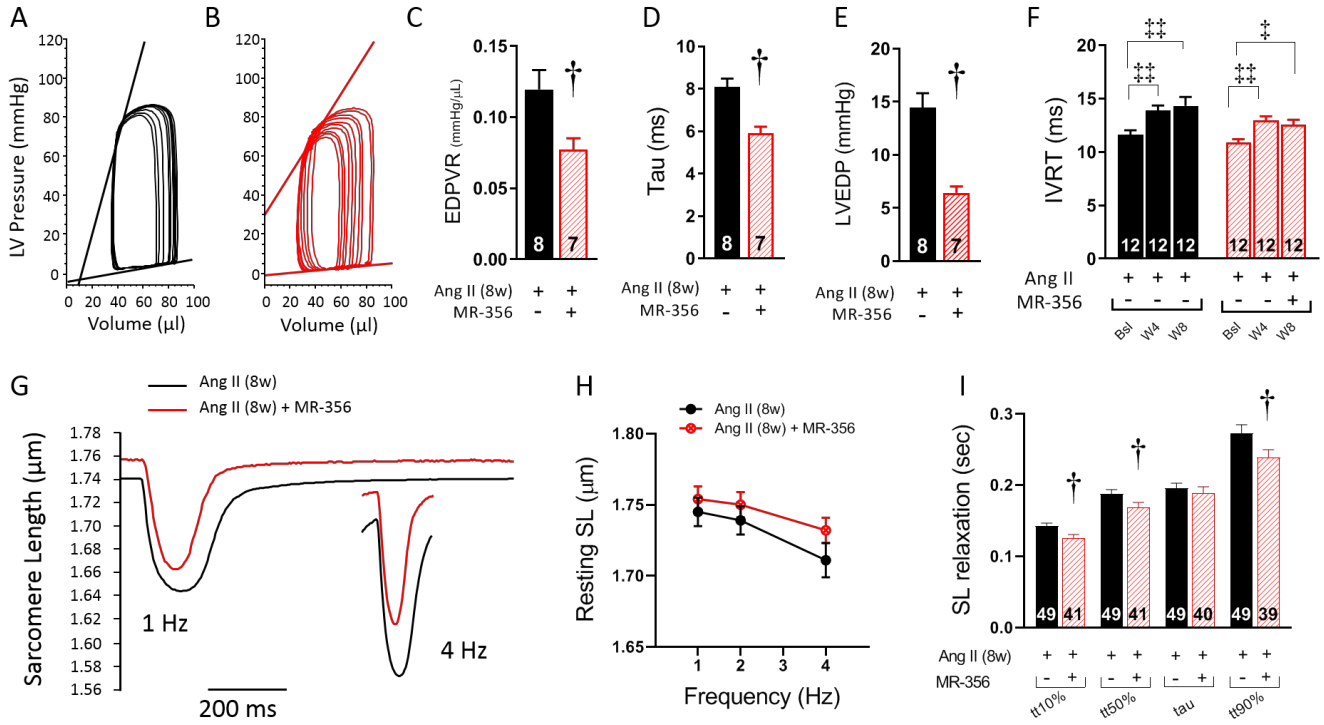

Figure 7: Effect of the GHRH-A MR-356 on the chronically installed HFpEF phenotype. (A) Representative pressure-volume (P-V) loops showing the linear regression for end-systolic pressure-volume relationship (ESPVR) and end-diastolic pressure-volume relationship (EDPVR) in a mouse treated for 8 weeks with Ang-II, or (B) an Ang-II (8w)+MR-356-treated mouse. (C) Averaged slopes from the EDPVR linear fitting. (D) Hemodynamic assessment of the relaxation time constant (tau) at 8-week time point. (E) Averaged left ventricular end-diastolic pressure (LVEDP). (F) Isovolumetric relaxation time (IVRT) as measured by transthoracic echocardiography at baseline, 4-week and 8-week. (G) Representative SL traces comparing Ang-II (8w)-treated and Ang-II (8w) + MR-356 cardiomyocytes at 1 and 4 Hz pacing rates. (H) Resting sarcomere length of Ang-II (8w)-treated compared with Ang-II (8w) + MR-356-treated mouse cardiomyocytes paced at 1, 2 and 4 Hz. (I) Averaged times to different degrees of SL relaxation: time to 10% (tt10%), time to 50% (tt50%), relaxation time constant (τ) and time to 90% (tt90%) in 8-week-treated cardiomyocytes paced at 1 Hz. † $p<0.05$ vs. Ang-II (8w)+ MR-356-treated; Student's t-test. ‡ $p<0.05$ within group comparison, two-way ANOVA.